


## Dirac semimetal in type-IV magnetic space groups

Guiyuan Hua,<sup>1,\*</sup> Simin Nie,<sup>2,\*</sup> Zhida Song,<sup>3,†</sup> Rui Yu,<sup>4,‡</sup> Gang Xu,<sup>1,§</sup> and Kailun Yao<sup>1</sup><sup>1</sup>Wuhan National High Magnetic Field Center and School of Physics, Huazhong University of Science and Technology, Wuhan 430074, China<sup>2</sup>Department of Materials Science and Engineering, Stanford University, Stanford, California 94305, USA<sup>3</sup>Beijing National Research Center for Condensed Matter Physics, and Institute of Physics, Chinese Academy of Sciences, Beijing 100190, China<sup>4</sup>School of Physics and Technology, Wuhan University, Wuhan 430072, China (Received 14 March 2018; revised manuscript received 25 October 2018; published 30 November 2018)

Analogs of the elementary particles, Dirac fermions in condensed matter, have received extensive attention for both scientific interest and device applications. In this Rapid Communication, we study the Dirac semimetals (DSMs) in the magnetic space groups (MSGs), and find a category of DSMs in centrosymmetric type-IV MSGs, where the Dirac points (DPs) are protected by inversion symmetry, nonsymmorphic time-reversal symmetry, and suitable rotation symmetry. Moreover, we propose the interlayer antiferromagnetic (AFM) material  $\text{EuCd}_2\text{As}_2$  as a promising candidate hosting only one pair of such DPs at the Fermi level. Many exotic topological states, such as the AFM triple-point semimetal, an AFM topological insulator exhibiting the half-quantum Hall effect, can be derived from such AFM DSMs by breaking certain symmetry. Our results extend the range of DSMs, and provide a platform to study the topological phase transition and the exotic properties of AFM topological states.

DOI: [10.1103/PhysRevB.98.201116](https://doi.org/10.1103/PhysRevB.98.201116)

Massless Dirac fermions (DFs) are one kind of the long-pursued elementary particles [1,2]. While their existence remains elusive in particle physics, the realization of DFs in Dirac semimetals (DSMs) [3–12] has received extensive attention for both scientific interest and device applications [13]. In three-dimensional (3D) materials with both time-reversal symmetry  $\mathcal{T}$  and inversion symmetry  $\mathcal{P}$ , each band energy is doubly degenerate. If two doubly degenerate bands linearly cross each other at a discrete momentum point, such a fourfold degenerate point is called the Dirac point [14], whose low-energy excitation can be described by a massless relativistic Dirac equation. Following such guidelines, several 3D DSMs have been proposed and confirmed experimentally in nonmagnetic systems [4–6,15–19].

Generally, both time-reversal symmetry and inversion symmetry are necessary to protect such fourfold degenerate Dirac points (DPs) in nonmagnetic materials. Otherwise, the system will evolve into other exotic quantum states such as Weyl semimetals [20–32] or topological insulators (TIs) [33]. However, an exception was recently proposed in a specific antiferromagnetic (AFM) configuration of  $\text{CuMnAs}$  [34], in which both  $\mathcal{P}$  and  $\mathcal{T}$  are broken but their combined  $\mathcal{PT}$  is preserved, so that Kramer's degeneracy is reserved for the generic momentum  $k$ , and DPs can exist in such a kind of AFM system. Thence, a natural question is whether there exist other types of DSMs in magnetic materials.

In the present Rapid Communication, we find that the concept of DSM can be generalized to centrosymmetric type-IV magnetic space groups (MSGs) that break  $\mathcal{T}$  but preserve  $\mathcal{P}$

and nonsymmorphic time-reversal symmetry  $\mathcal{T}' = \mathcal{T}\tau$ , where  $\tau$  is a fractional translation operator that connects the black and white Bravais lattices. Guided by this idea, a concrete example of such a DSM, the interlayer AFM  $\text{EuCd}_2\text{As}_2$ , is predicted by density functional theory (DFT) calculations. Many exotic topological states can be derived from such an AFM DSM. When threefold rotation symmetry  $C_{3z}$  is broken, the DSM phase can evolve into an AFM TI phase exhibiting the half-quantum Hall effect on the (001) surface as discussed by Moore *et al.* [35]. In the case of breaking  $\mathcal{P}$ , an AFM triple-point semimetal, rather than a Weyl semimetal, can be stabilized. Our results extend the range of DSM, and provide one candidate to study the DSM and other exotic AFM topological states.

*Types of DSMs in type-IV MSGs.* In order to search for different types of DSMs, we have checked all types of MSGs. The Kramer's degeneracy at a generic momentum  $k$  is an essential requirement for the realization of DPs in solids. Therefore, any MSG that may host DPs should contain time-reversal operation  $\mathcal{T}$  (or its combined operation), which is the premise condition of Kramer's degeneracy. According to Ref. [36], there is no  $\mathcal{T}$  presenting in type-I MSGs, where MSGs  $\mathcal{M}$  are defined as ordinary space group  $\mathcal{G}$  ( $\mathcal{M} = \mathcal{G}$ ). So, the DSM phase can never exist in type-I MSGs. In type-II MSGs,  $\mathcal{M}$  are defined as  $\mathcal{G} + \mathcal{T}\mathcal{G}$ . These MSGs are actually the space groups plus the time-reversal operation, in which the classification of all kinds of DSM phases has been discussed by Nagaosa *et al.* [8]. In type-III MSGs,  $\mathcal{M}$  are defined as  $\mathcal{H} + \mathcal{T}(\mathcal{G} - \mathcal{H})$ , where  $\mathcal{H}$  is a halving subgroup of the space group  $\mathcal{G}$  and  $(\mathcal{G} - \mathcal{H})$  contains no pure translations. In this case, the DPs can only exist in type-III MSGs that contain the combined operator  $\mathcal{PT}$ . The AFM DSM  $\text{CuMnAs}$  discussed by Tang *et al.* [34] belongs to this situation. In type-IV MSGs,  $\mathcal{M}$  are defined as  $\mathcal{G} + \mathcal{T}\{\epsilon|\tau\}\mathcal{G}$ , where  $\epsilon$  is the identity operation and  $\tau$  is the extra translation connecting the black

\*These authors contributed equally to this work.

†song.zhida@iphy.ac.cn

‡yurui@whu.edu.cn

§gangxu@hust.edu.cn

(up-spin) and white (down-spin) sublattices. Obviously, there is no pure time-reversal operation in type-IV MSGs. The operation that changes the direction of the spin moment in type-IV MSGs becomes a nonsymmorphic form  $\mathcal{T}' = \mathcal{T}\tau$ . We call  $\mathcal{T}'$  nonsymmorphic time-reversal symmetry to distinguish from ordinary time-reversal symmetry  $\mathcal{T}$ .

It is easy to identify that the representation of  $\mathcal{T}'$  in the momentum space satisfies  $\mathcal{T}'^2 = \mathcal{T}\tau\mathcal{T}\tau = -\tau^2 = -e^{2ik\cdot\tau}$ , and itself cannot ensure Kramer's degeneracy in the whole momentum space. Fortunately, we find that the combination of  $\mathcal{T}'$  and  $\mathcal{P}$ , i.e.,  $\mathcal{P}\mathcal{T}'$ , whose square equals  $-1$  [ $(\mathcal{P}\mathcal{T}')^2 = \mathcal{P}\mathcal{T}'\mathcal{P}\mathcal{T}' = \mathcal{P}\mathcal{T}\mathcal{P}(-\tau)\mathcal{T}\tau = \mathcal{P}^2\mathcal{T}^2e^{-ik\cdot\tau}e^{ik\cdot\tau} = -1$ ], is a sufficient condition to protect Kramer's degeneracy at the generic momentum  $k$ . Therefore, we will focus on centrosymmetric type-IV MSGs that contain both  $\mathcal{T}'$  and  $\mathcal{P}$  in the following, which may support the DSM phase.

In addition to the symmetry  $\mathcal{T}'$  and  $\mathcal{P}$ , a suitable crystal symmetry, such as rotation symmetry  $C_n$ , is also needed to protect stable DPs in centrosymmetric type-IV MSGs. Therefore, there are only two classes of locations that DPs can exist in the momentum space: DPs on the rotation axis away from the time-reversal invariant momentum (TRIM) points (class I) and DPs on the TRIM points (class II). In the presence of  $\mathcal{P}$ ,  $\mathcal{T}'$ , and  $C_n$  ( $n = 3, 4, \text{ or } 6$ ), the classification of class-I DSMs in centrosymmetric type-IV MSGs is homologous to the discussion given by Nagaosa *et al.* [8], because the small group of  $k$  points on the rotation momentum axis is isomorphic with that in type-II MSGs, both satisfying  $C_n^n = -1$ ,  $(\mathcal{P}\mathcal{T}')^2 = -1$ , and  $[C_n, \mathcal{P}\mathcal{T}'] = 0$ . As an illustrative example of a class-I DSM in type-IV MSGs, the interlayer AFM  $\text{EuCd}_2\text{As}_2$  will be addressed in this Rapid Communication, and its derivative exotic states, such as the AFM TI and triple-point semimetal, will be discussed, too.

Considering the representation  $\mathcal{T}'^2 = -e^{2ik\cdot\tau}$ , two cases of TRIM points need to be differentiated depending on the value of  $k \cdot \tau$ : case 1, TRIM points with  $k \cdot \tau = 0$  or  $\pi$ ; and case 2, TRIM points with  $k \cdot \tau = \pi/2$ . For case 1, the algebraic relations of  $\mathcal{P}$  and  $\mathcal{T}'$  are similar to the discussion in Ref. [8], satisfying  $\mathcal{P}^2 = 1$ ,  $\mathcal{T}'^2 = -1$ , and  $[\mathcal{P}, \mathcal{T}'] = 0$ . When rotation symmetry  $C_n$  ( $n = 2, 4, 6$ ) is present, a single DP can be stabilized at the TRIM points of case 1, because their small group in type-IV MSGs is isomorphic with that in type-II MSGs, i.e.,  $\{C_n, \mathcal{P}\} = 0$  and  $[C_n, \mathcal{T}'] = 0$ . However, for the TRIM points with  $k \cdot \tau = \pi/2$  (case 2), the algebraic relations between  $\mathcal{P}$  and  $\mathcal{T}'$  are different and particular,  $\mathcal{P}^2 = 1$ ,  $\mathcal{T}'^2 = 1$ ,  $\{\mathcal{P}, \mathcal{T}'\} = 0$ , and  $(\mathcal{P}\mathcal{T}')^2 = -1$ , where the minus sign of  $(\mathcal{P}\mathcal{T}')^2$  comes from the anticommutative relation  $\{\mathcal{P}, \mathcal{T}'\} = 0$ . These algebraic relations are now being addressed in the fermion system, so the conclusion in Ref. [8] is not applicable now. In this Rapid Communication, we provide proof that these algebraic relations prohibit all kinds of DPs with odd-order dispersions in type-IV MSGs. The general discussions of their topological character are left for future work.

Let us begin by assuming a fourfold band degeneracy located at the case 2 TRIM points. Without loss of generality, one can write the four-dimensional  $\mathcal{T}' = \tau_0\sigma_x K$ ,  $\mathcal{P} = \tau_0\sigma_z$ ,  $\mathcal{P}\mathcal{T}' = i\tau_0\sigma_y K$ , where  $\tau_0$  indicates the two-dimensional identity matrix for the orbital basis,  $\sigma_{x,y,z}$  are the Pauli matrices describing spin degrees of freedom, and  $K$  is the complex conjugation operator. It is obvious that, besides the identity matrix

$\tau_0\sigma_0$ , only the following five  $\gamma$  matrices, i.e.,  $\sigma_0\tau_x$ ,  $\sigma_0\tau_z$ ,  $\sigma_x\tau_y$ ,  $\sigma_z\tau_y$ ,  $\sigma_y\tau_y$ , can be used to construct the Hamiltonian yielding the requirement  $[H(k), \mathcal{P}\mathcal{T}'] = 0$ , where  $H(k) = \sum_{i=1,5} f_i(k)\gamma_i$ , and  $f_i(k)$  are real functions of  $k$ . Furthermore, due to the requirement of  $\mathcal{P}H(k)\mathcal{P}^{-1} = H(-k)$ , only two  $\gamma$  matrices,  $\sigma_x\tau_y$  and  $\sigma_y\tau_y$ , which anticommute with  $\mathcal{P} = \tau_0\sigma_z$ , could couple to the odd-type function  $f(k)$ . On the other hand, to get a linear DP, we need three such kinds of  $\gamma$  matrices. To leading order, the effective Hamiltonian around the DP can be written as  $H = \sum_{i,j}^3 k_i A_{ij} \gamma_j$  and the dispersion is given by  $E(k) = \pm\sqrt{\sum_j^3 (\sum_i^3 k_i A_{ij})^2}$ . Here,  $A$  is a  $3 \times 3$  matrix with full rank. If we have only two (or one) such  $\gamma$  matrices, or, equivalently,  $A$  is a rank-2 (rank-1) matrix, then the velocity of dispersion must vanish along one (two) particular direction(s), which can be indicated by the zero eigenvector(s) of  $A$ . Similarly, it can be proved that all kinds of odd-order DPs cannot exist at the case 2 TRIM points in type-IV MSGs, and this conclusion does not depend on the representation choice of  $\mathcal{T}'$  and  $\mathcal{P}$ .

**AFM DSM  $\text{EuCd}_2\text{As}_2$ .** Guided by the DSM classification in the type-IV MSGs, we discover that a pair of class-I DPs (belonging to type-IV MSGs) can be hosted at the Fermi level in the interlayer AFM  $\text{EuCd}_2\text{As}_2$ . As shown in Fig. S1a,  $\text{EuCd}_2\text{As}_2$  crystallizes into the  $\text{CaAl}_2\text{Si}_2$ -type structure with space group  $D_{3d}^3$  ( $P\bar{3}m1$ ) [37–39], in which  $\text{Cd}_2\text{As}_2$  layers are separated by the trigonal Eu layers. Here, the projector augmented-wave method implemented in the Vienna *ab initio* simulation package is employed to carry out the DFT calculations [40–42]. All results are cross checked with the full-potential linearized-augmented plane-wave method implemented in the WIEN2K package. Considering that  $\text{Eu}^{2+}$  has a half-filled  $4f$  shell, we have calculated three different magnetic configurations for  $\text{EuCd}_2\text{As}_2$  by the generalized gradient approximation (GGA)+Hubbard- $U$  (GGA+ $U$ ) method [43] with  $U = 5$  eV, including the ferromagnetic (FM), frustrated AFM, and interlayer AFM configurations as shown in Figs. S1a, S1b, and S1c, respectively. All the magnetic moments proposed here are assumed along the  $c$  direction, which is in small contrast to recent observations [44]. This is because  $\text{EuCd}_2\text{As}_2$  is a very soft magnet [44]. Our calculations indicate that it is easy to change its moment direction by enlarging the in-plane lattice constant. More details and discussions of the magnetic anisotropy are presented in the Supplemental Material [45]. The calculated total energies and moments are summarized in Table S1. Our calculations demonstrate that all magnetic states are lower than the nonmagnetic state about 6.3 eV/f.u., and the interlayer AFM is the most stable one, further lowering the total energy about 2 meV/f.u. than the ferromagnetic states, which are very consistent with a recent experimental measurement [46].

The projected band structures of the interlayer AFM  $\text{EuCd}_2\text{As}_2$  are shown in Fig. 1(a). Our DFT calculations indicate that the low-energy bands near the Fermi level are mainly contributed from the  $p$  orbitals of As atoms and the  $s$  orbitals of the Cd atoms. In particular, the doubly degenerate  $s$ - $s$  bonding states of Cd atoms (even parity) invert with the  $p$ - $p$  antibonding states of As atoms (odd parity) at the Fermi level around the  $\Gamma$  point. At first glance, it is a little surprising that the crossing along the  $\Gamma$ - $A$  line has no gap

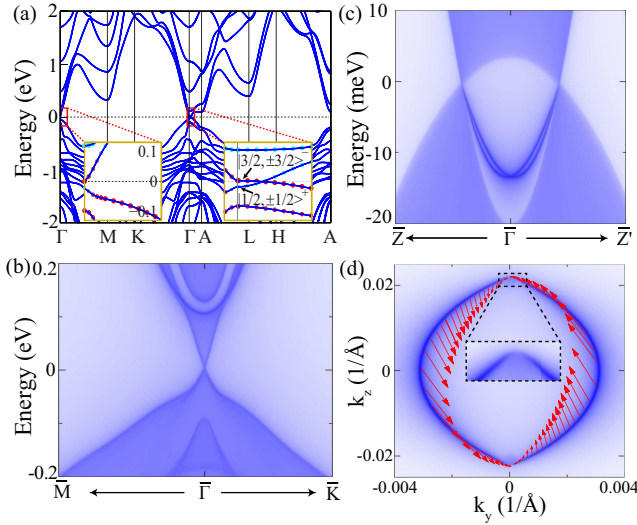


FIG. 1. The electronic structure in the interlayer AFM  $\text{EuCd}_2\text{As}_2$ . (a) The GGA+ $U$ +SOC calculated band structures of the interlayer AFM  $\text{EuCd}_2\text{As}_2$ . The insets are the zoom-in of the band structures around the  $\Gamma$  point to clearly show the DP, where the red and the light blue dots represent the projections of the As  $p$  and Cd  $s$  orbitals, respectively. (b) and (c) are the calculated surface states of the interlayer AFM  $\text{EuCd}_2\text{As}_2$  on the (001) and (100) faces, respectively. (d) The Fermi arcs and their spin textures on the (100) face of the interlayer AFM  $\text{EuCd}_2\text{As}_2$ , where the inset reveals the discontinuity at the DPs between two Fermi arcs.

but a stable fourfold degenerate DP, because  $\mathcal{T}$  is broken. However, after a detailed symmetry analysis, one can find that a nonsymmorphic time-reversal symmetry  $\mathcal{T}' = \mathcal{T} \oplus c$ , connecting the up-spin momentum layer at  $z = 0$  and the down-spin momentum layer at  $z = c$ , exists in this interlayer AFM system. The MSGs of the interlayer AFM  $\text{EuCd}_2\text{As}_2$  can be expressed as  $D_{3d}^4 \oplus \mathcal{T}' D_{3d}^4$ , whose generators include  $\mathcal{T}'$ ,  $\mathcal{P}$ ,  $C_{3z}$ , and twofold screw  $C_{2x}' = C_{2x} \oplus c$ . Combining  $\mathcal{T}' = \mathcal{T} \oplus c$  with  $\mathcal{P}$ , the antiunitarity of  $\mathcal{P}\mathcal{T}'$  would prohibit the hopping terms between the nonsymmorphic time-reversal pair of states, such as  $|3/2, \pm 3/2\rangle$  or  $|1/2, \pm 1/2\rangle$ , so that every energy state is doubly degenerate in such an interlayer AFM system. As we discussed above, it is possible to host the DPs with the help of proper rotation symmetry, which is exactly what happens on the  $\Gamma$ - $A$  line in the interlayer AFM  $\text{EuCd}_2\text{As}_2$ .

The small group of  $k$  points on the  $\Gamma$ - $A$  line can be described as  $C_{3v} \oplus \mathcal{P}\mathcal{T}'C_{3v}$ . When spin-orbit coupling (SOC) is included, the topology of the system and the band inversion are dominated by the four states  $|3/2, \pm 3/2\rangle^-$  from the  $p$ - $p$  antibonding states of As and  $|1/2, \pm 1/2\rangle^+$  from the  $s$ - $s$  bonding states of Cd. Under symmetry restrictions, an effective  $4 \times 4$   $k \cdot p$  model (in the order of  $|1/2, 1/2\rangle^+$ ,  $|3/2, 3/2\rangle^-$ ,  $|1/2, -1/2\rangle^+$ ,  $|3/2, -3/2\rangle^-$ ) around the  $\Gamma$  point can be written as Eq. (S1) in the Supplemental Material. By diagonalizing the above Hamiltonian, two linear DPs at  $k^c = (0, 0, \pm\sqrt{M_0/M_1})$  can be obtained on the  $\Gamma$ - $A$  line, where  $M_0$  and  $M_1$  are two real parameters and defined in the Supplemental Material [45]. This fact is confirmed by the calculated surface states [Figs. 1(b) and 1(c)] and Fermi arcs

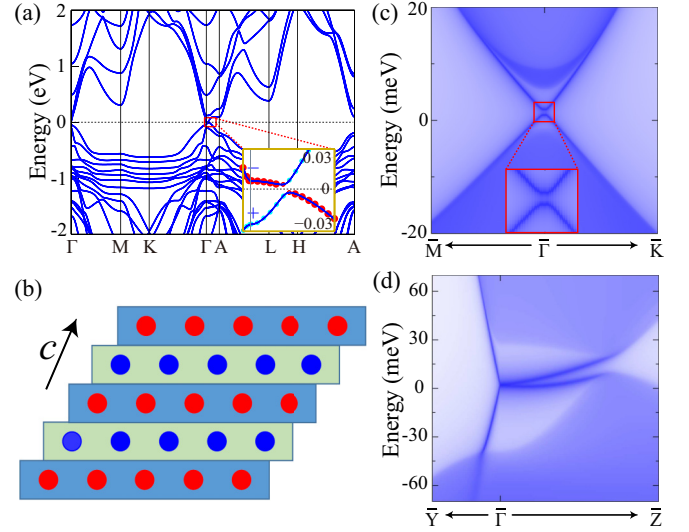


FIG. 2. The derivative exotic topological states from the AFM DSM  $\text{EuCd}_2\text{As}_2$  by breaking  $C_{3z}$ . (a) The GGA+ $U$ +SOC calculated band structures of the interlayer AFM  $\text{EuCd}_2\text{As}_2$  in the case of  $C_{3z}$  breaking. The insets are the zoom-in of band structures along the  $\Gamma$ - $A$  direction to exhibit the insulating gap. (b) Schematic of the AFM TI by stacking the 2D Chern insulators along the  $c$  axis, where the red and blue balls represent the up-spin layers (Chern number  $C = 1$ ) and down-spin layers ( $C = -1$ ), respectively. (c), (d) The calculated surface states of the AFM TI on the (001) and (100) faces, respectively. The inset of (c) shows the intrinsic gapped surface states clearly.

[Fig. 1(d)] based on the Green's functions of the semi-infinite system, which are constructed by the maximally localized Wannier functions [47,48]. The (001) surface states plotted in Fig. 1(b) exhibit a clear band touching at the  $\Gamma$  point and Fermi level, where a pair of DPs are projected to the same point on the (001) face. More evidence supporting the DSM phase comes from the Fermi arcs on the (010) face as plotted in Figs. 1(c) and 1(d), where a pair of arc states unambiguously connect the DPs from the bulk state. As shown in the inset of Fig. 1(d), even though the Fermi arcs appear to be closed, their Fermi velocities are discontinuous at the DPs. Such types of closed Fermi arcs in DSMs have been discussed by Wang *et al.* [5] and Tang *et al.* [34].

*TI phase and triple-point semimetal in AFM system.* In addition to the generic features discussed above, our AFM DSM has its own uniqueness. Such a uniqueness can be reflected by its derivatives, which makes our AFM DSM different from  $\text{Na}_3\text{Bi}$  and  $\text{CuMnAs}$ .

First, we would like to discuss the derivative TI phase from the AFM DSM  $\text{EuCd}_2\text{As}_2$ . As discussed above,  $C_{3z}$  is important for the stability of the DPs in the interlayer AFM  $\text{EuCd}_2\text{As}_2$ . When this symmetry is broken,  $j_z$  is no longer a good quantum number on the  $\Gamma$ - $A$  line, so that the hopping terms between  $|j_z = \pm 1/2\rangle$  and  $|j_z = \pm 3/2\rangle$  can be introduced, and the system evolves into a strong TI phase due to the inverted band structure. One can achieve this object by applying uniaxial strain or by tuning the magnetic moment to the in-plane direction [44,45].

In Fig. 2(a), we plot the band structures by enlarging the  $a$  axis by 1%, where an insulating gap of 9 meV clearly opens

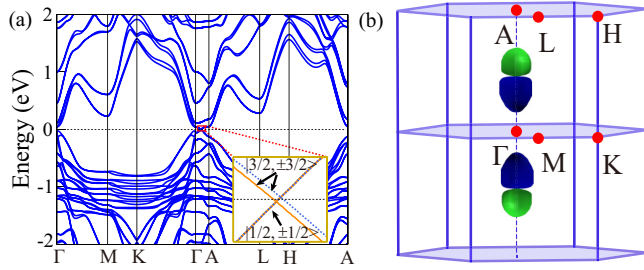


FIG. 3. The derivative exotic topological state from the AFM DSM  $\text{EuCd}_2\text{As}_2$  by breaking  $\mathcal{P}$ . (a) The GGA+ $U$ +SOC calculated band structures of the interlayer AFM  $\text{EuCd}_2\text{As}_2$  in the case of  $\mathcal{P}$  breaking (triple-point semimetal). The insets are the zoom-in of band structures along the  $\Gamma$ - $A$  direction to distinctly exhibit the triple points. (b) The calculated Fermi surfaces of a triple-point semimetal derived from the interlayer AFM  $\text{EuCd}_2\text{As}_2$  with  $\mathcal{P}$  breaking, where the Fermi surfaces are magnified 60 times to visibly exhibit them and their tangency.

up. The TI phase realized in Fig. 2(a) has unique topological properties. It is not a conventional 3D TI as  $\text{Bi}_2\text{Se}_3$ , but the AFM TI protected by  $\mathcal{T}'$  as discussed by Moore *et al.* [35]. To illustrate the difference, one can see the (001) surface states plotted in Fig. 2(c), where the surface states are intrinsically gapped at the  $\bar{\Gamma}$  point, because  $\mathcal{T}'$  is broken when an open boundary is applied on the  $c$  axis. However, when an open boundary is applied to the other directions, such as the  $a$  axis, where  $\mathcal{T}'$  is preserved, the surface states remain gapless as that in a conventional TI [see Fig. 2(d)]. These characters conform exactly with the discussion of the AFM TI [35], which can be taken as a product state of the two-dimensional (2D) Chern insulators stacked along the  $c$  axis, and each pair of nearest neighbors are connected by  $\mathcal{T}' = \mathcal{T} \oplus c$  [Fig. 2(b)]. Therefore, a nontrivial AFM  $\mathbb{Z}_2$  invariant related to  $\mathcal{T}'$  can be defined, and the half-quantum Hall effect can be realized on the intrinsically gapped (001) face of such an AFM TI [35] [Fig. 2(c)].

The other big difference between our AFM DSM and the other DSMs ( $\text{Na}_3\text{Bi}$  and  $\text{CuMnAs}$ ) can be reflected by breaking  $\mathcal{P}$ . As we all know, the DPs usually split into two pairs of Weyl points with opposite chirality in a conventional DSM when  $\mathcal{P}$  is broken. However, two pairs of triple points protected by the small  $C_{3v}$  group (consisting of  $C_{3z}$  and  $M_x$ ) are obtained in our AFM DSM when  $\mathcal{P}$  is broken. Such results are plotted in Fig. 3(a), in which  $|j_z = \pm 3/2\rangle$  states are split, while the  $|j_z = \pm 1/2\rangle$  states remain doubly degenerate.

The origin of the triple-point semimetal realized in the  $\mathcal{P}$  breaking  $\text{EuCd}_2\text{As}_2$  can be understood as follows. In the absence of  $\mathcal{PT}'$  symmetry, the small group of  $k$  points on  $\Gamma$ - $A$  reduces to the magnetic point group  $C_{3v}$ , which has one 2D irreducible representation  $E_{1/2}$  ( $|\pm 1/2\rangle$ ) and two one-dimensional irreducible representations  $E_{3/2}$  ( $\frac{1}{\sqrt{2}}|\pm 3/2\rangle \pm \frac{i}{\sqrt{2}}|\pm 3/2\rangle$ ). Therefore, the degeneracy between  $|\pm 3/2\rangle$  states, which is originally protected by  $\mathcal{PT}'$ , is broken, while the degeneracy between  $|\pm 1/2\rangle$  remains, naturally leading to two pairs of triple points on the  $\Gamma$ - $A$  line. We calculate the Fermi surfaces of the triple-point semimetal phase and plot them in Fig. 3(b), where two pairs of tangent Fermi pockets exist, and each pocket encloses one triple point. Similar to the nonmagnetic triple-point semimetal [49–51], two touching Fermi pockets hold opposite spin winding numbers. Finally, it is worth noting that we are reporting a triple-point semimetal in a magnetic material. The topological property of such a magnetic topological material is usually related to the specific magnetic order, which provides a mechanism to tune the topological phase transition by changing the magnetic order or the external magnetic field.

*Conclusion.* In summary, we generalized the concept of DSM to centrosymmetric type-IV MSGs, where the antiunitarity of the product between  $\mathcal{P}$  and  $\mathcal{T}'$ , i.e.,  $(\mathcal{PT}')^2 = -1$ , is essential for Kramer's degeneracy and the AFM DPs. Based on DFT calculations, we propose that the interlayer AFM  $\text{EuCd}_2\text{As}_2$  is a candidate for such an AFM DSM. Many exotic topological states can be derived from the AFM DSMs. For example, when threefold rotation symmetry is broken, it can evolve into the AFM TI discussed by Moore *et al.* [35], where the half-quantum Hall effect can be realized on the intrinsically gapped (001) face. If  $\mathcal{P}$  is broken, it can result in a triple-point semimetal phase, rather than a Weyl semimetal. Our results provide a direction to study the DSM and other exotic AFM topological states.

*Note added.* Recently, we became aware of evidence of a Dirac-cone type dispersion in  $\text{EuCd}_2\text{As}_2$  that has been observed in the angle-resolved photoemission spectroscopy (ARPES) measurements by Ma *et al.* [52], which greatly supports our theoretical predictions.

*Acknowledgments.* We thank Tian Qian and Yulin Chen for useful discussions. This work is supported by the Ministry of Science and Technology of China (2018YFA0307000); G.X. and R.Y. are supported by the National Thousand-Young-Talents Program and the National Natural Science Foundation of China (11874022); S.N. is supported by Stanford Energy 3.0.

- [1] H. Weyl, *Z. Phys.* **56**, 330 (1929).
- [2] G. E. Volovik, *The Universe in a Helium Droplet*, Vol. 117 (Oxford University Press, Oxford, U.K., 2003).
- [3] S. Murakami, *New J. Phys.* **9**, 356 (2007).
- [4] S. M. Young, S. Zaheer, J. C. Y. Teo, C. L. Kane, E. J. Mele, and A. M. Rappe, *Phys. Rev. Lett.* **108**, 140405 (2012).
- [5] Z. Wang, Y. Sun, X.-Q. Chen, C. Franchini, G. Xu, H. Weng, X. Dai, and Z. Fang, *Phys. Rev. B* **85**, 195320 (2012).
- [6] Z. Wang, H. Weng, Q. Wu, X. Dai, and Z. Fang, *Phys. Rev. B* **88**, 125427 (2013).
- [7] O. Vafek and A. Vishwanath, *Annu. Rev. Condens. Matter Phys.* **5**, 83 (2014).
- [8] B.-J. Yang and N. Nagaosa, *Nat. Commun.* **5**, 4898 (2014).
- [9] S. M. Young and B. J. Wieder, *Phys. Rev. Lett.* **118**, 186401 (2017).
- [10] B. Bradlyn, L. Elcoro, J. Cano, M. G. Vergniory, Z. Wang, C. Felser, M. I. Aroyo, and B. A. Bernevig, *Nature (London)* **547**, 298 (2017).
- [11] H. C. Po, A. Vishwanath, and H. Watanabe, *Nat. Commun.* **8**, 50 (2017).

- [12] H. C. Watanabe, H. Po, and A. Vishwanath, *Sci. Adv.* **4**, eaat8685 (2018).
- [13] M. Koshino and T. Ando, *Phys. Rev. B* **81**, 195431 (2010).
- [14] A. Burkov, *Nat. Mater.* **15**, 1145 (2016).
- [15] Z. Liu, B. Zhou, Y. Zhang, Z. Wang, H. Weng, D. Prabhakaran, S.-K. Mo, Z. Shen, Z. Fang, X. Dai *et al.*, *Science* **343**, 864 (2014).
- [16] S. Borisenko, Q. Gibson, D. Evtushinsky, V. Zabolotnyy, B. Büchner, and R. J. Cava, *Phys. Rev. Lett.* **113**, 027603 (2014).
- [17] J. Xiong, S. K. Kushwaha, T. Liang, J. W. Krizan, M. Hirschberger, W. Wang, R. Cava, and N. Ong, *Science* **350**, 413 (2015).
- [18] M. Novak, S. Sasaki, K. Segawa, and Y. Ando, *Phys. Rev. B* **91**, 041203 (2015).
- [19] J. A. Steinberg, S. M. Young, S. Zaheer, C. L. Kane, E. J. Mele, and A. M. Rappe, *Phys. Rev. Lett.* **112**, 036403 (2014).
- [20] X. Wan, A. M. Turner, A. Vishwanath, and S. Y. Savrasov, *Phys. Rev. B* **83**, 205101 (2011).
- [21] G. Xu, H. Weng, Z. Wang, X. Dai, and Z. Fang, *Phys. Rev. Lett.* **107**, 186806 (2011).
- [22] H. Weng, C. Fang, Z. Fang, B. A. Bernevig, and X. Dai, *Phys. Rev. X* **5**, 011029 (2015).
- [23] S.-M. Huang, S.-Y. Xu, I. Belopolski, C.-C. Lee, G. Chang, B. Wang, N. Alidoust, G. Bian, M. Neupane, C. Zhang *et al.*, *Nat. Commun.* **6**, 7373 (2015).
- [24] S.-Y. Xu, I. Belopolski, N. Alidoust, M. Neupane, G. Bian, C. Zhang, R. Sankar, G. Chang, Z. Yuan, C.-C. Lee *et al.*, *Science* **349**, 613 (2015).
- [25] B. Lv, H. Weng, B. Fu, X. Wang, H. Miao, J. Ma, P. Richard, X. Huang, L. Zhao, G. Chen *et al.*, *Phys. Rev. X* **5**, 031013 (2015).
- [26] B. Lv, S. Muff, T. Qian, Z. Song, S. Nie, N. Xu, P. Richard, C. Matt, N. Plumb, L. Zhao *et al.*, *Phys. Rev. Lett.* **115**, 217601 (2015).
- [27] C. Wang, Y. Zhang, J. Huang, S. Nie, G. Liu, A. Liang, Y. Zhang, B. Shen, J. Liu, C. Hu *et al.*, *Phys. Rev. B* **94**, 241119(R) (2016).
- [28] L. Yang, Z. Liu, Y. Sun, H. Peng, H. Yang, T. Zhang, B. Zhou, Y. Zhang, Y. Guo, M. Rahn *et al.*, *Nat. Phys.* **11**, 728 (2015).
- [29] Y. Sun, S.-C. Wu, and B. Yan, *Phys. Rev. B* **92**, 115428 (2015).
- [30] Y. Sun, S.-C. Wu, M. N. Ali, C. Felser, and B. Yan, *Phys. Rev. B* **92**, 161107 (2015).
- [31] A. Liang, J. Huang, S. Nie, Y. Ding, Q. Gao, C. Hu, S. He, Y. Zhang, C. Wang, B. Shen *et al.*, [arXiv:1604.01706](https://arxiv.org/abs/1604.01706).
- [32] S. Nie, G. Xu, F. B. Prinz, and S.-c. Zhang, *Proc. Natl. Acad. Sci. U.S.A.* **114**, 10596 (2017).
- [33] H.-J. Zhang, S. Chadov, L. Müchler, B. Yan, X.-L. Qi, J. Kübler, S.-C. Zhang, and C. Felser, *Phys. Rev. Lett.* **106**, 156402 (2011).
- [34] P. Tang, Q. Zhou, G. Xu, and S.-C. Zhang, *Nat. Phys.* **12**, 1100 (2016).
- [35] R. S. K. Mong, A. M. Essin, and J. E. Moore, *Phys. Rev. B* **81**, 245209 (2010).
- [36] C. Bradley and A. Cracknell, *The Mathematical Theory of Symmetry in Solids: Representation Theory for Point Groups and Space Groups* (Oxford University Press, Oxford, U.K., 2010).
- [37] A. Artmann, A. Mewis, M. Roepke, and G. Michels, *Z. Anorg. Allg. Chem.* **622**, 679 (1996).
- [38] Y. Goryunov, V. Fritsch, H. v. Löhneysen, and A. Nateprov, *J. Phys.: Conf. Ser.* **391**, 012015 (2012).
- [39] I. Schellenberg, M. Eul, W. Hermes, and R. Pöttgen, *Z. Anorg. Allg. Chem.* **636**, 85 (2010).
- [40] G. Kresse and J. Furthmüller, *Comput. Mater. Sci.* **6**, 15 (1996).
- [41] G. Kresse and J. Furthmüller, *Phys. Rev. B* **54**, 11169 (1996).
- [42] J. P. Perdew, K. Burke, and M. Ernzerhof, *Phys. Rev. Lett.* **77**, 3865 (1996).
- [43] A. I. Liechtenstein, V. I. Anisimov, and J. Zaanen, *Phys. Rev. B* **52**, R5467(R) (1995).
- [44] M. C. Rahn, J.-R. Soh, S. Francoual, L. S. I. Veiga, J. Stempffer, J. Mardegan, D. Y. Yan, Y. F. Guo, Y. G. Shi, and A. T. Boothroyd, *Phys. Rev. B* **97**, 214422 (2018).
- [45] See Supplemental Material at <http://link.aps.org/supplemental/10.1103/PhysRevB.98.201116> for the details on the crystal structure and magnetic structure of  $\text{EuCd}_2\text{As}_2$ , the  $k \cdot p$  model of  $\text{EuCd}_2\text{As}_2$ , the magnetic anisotropy energy of  $\text{EuCd}_2\text{As}_2$ , and the AFM TI for  $\text{EuCd}_2\text{As}_2$  with in-plane  $A$ -AFM.
- [46] H. P. Wang, D. S. Wu, Y. G. Shi, and N. L. Wang, *Phys. Rev. B* **94**, 045112 (2016).
- [47] M. L. Sancho, J. L. Sancho, and J. Rubio, *J. Phys. F: Met. Phys.* **14**, 1205 (1984).
- [48] M. L. Sancho, J. L. Sancho, J. L. Sancho, and J. Rubio, *J. Phys. F: Met. Phys.* **15**, 851 (1985).
- [49] Z. Zhu, G. W. Winkler, Q. S. Wu, J. Li, and A. A. Soluyanov, *Phys. Rev. X* **6**, 031003 (2016).
- [50] H. Weng, C. Fang, Z. Fang, and X. Dai, *Phys. Rev. B* **94**, 165201 (2016).
- [51] H. Weng, C. Fang, Z. Fang, and X. Dai, *Phys. Rev. B* **93**, 241202 (2016).
- [52] J. Ma *et al.* (private communication).